IEEE Photonics Journal
An IEEE Photonics Society Publication

Open Access

Improved ADRC With ILC Control of a CCD-Based Tracking Loop for Fast Steering Mirror System

Volume 10, Number 4, August 2018

Quanrui Dong
Yongkai Liu
Yuliang Zhang
Shijie Gao
Tao Chen

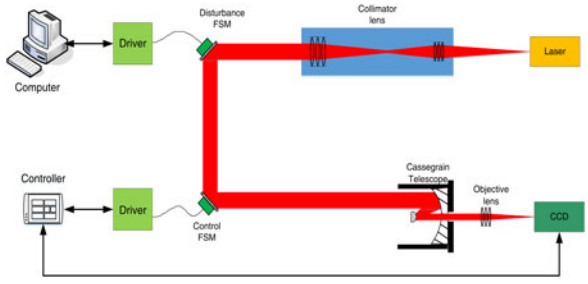

DOI: 10.1109/JPHOT.2018.2846287
1943-0655 © 2018 IEEE

IEEE photonics SOCIETY

IEEE

Improved ADRC With ILC Control of a CCD-Based Tracking Loop for Fast Steering Mirror System

Quanrui Dong,[1,2] **Yongkai Liu**,[1,2] **Yuliang Zhang**,[1] **Shijie Gao**,[1] **and Tao Chen**[1]

[1]Changchun Institute of Optics, Fine Mechanics and Physics, Chinese Academy of Sciences, Changchun 130033, China
[2]University of Chinese Academy of Sciences, Beijing 100049, China

DOI:10.1109/JPHOT.2018.2846287

Manuscript received May 2, 2018; revised June 2, 2018; accepted June 7, 2018. Date of publication June 11, 2018; date of current version July 4, 2018. This work was supported by Research project of scientific research equipment of Chinese Academy of Sciences (2017). Corresponding author: Yongkai Liu (e-mail: liuyongkai_ciomp@163.com).

Abstract: In order to improve the tracking accuracy of the fine tracking system of free-space optical communications, a proposed active disturbance rejection control (ADRC) with iterative learning control (ILC) strategy is designed to regulate the fast steering mirror (FSM) system. First, based on the open-loop frequency response results of the system, we can approximately confirm the system transfer function and prepare for the design of the controller. Then, an improved ADRC that using sliding mode control instead of the traditional nonlinear state error feedback method is proposed to attenuate the influence of the unknown and unmolded parts. In addition, the ILC method is used to compensate the hysteresis of piezoelectric actuators and improve the overall system performance. The experimental results indicate that the tracking accuracy of the system is 1 μrad at 1k sampling frequency. In addition, the recommended method shows the better disturbance suppression performance than traditional ADRC in simulation and experimental investigations. This method has a very high application value in the field of visual axis stability, adaptive optics, and other fields.

Index Terms: Fast steering mirror, disturbance suppression, active disturbance rejection control (ADRC), sliding mode control (SMC), iterative learning control (ILC).

1. Introduction

Fast steering mirrors (FSMs) are widely used in optical systems which include adaptive optics, long-distance FSO communications and line-of-sight (LOS) stabilization [1]–[4]. In this paper, FSMs are applied to the high precision positioning systems of FSO communications, which are driven by the piezoelectric actuators (PEAs). However, with the enhancement of maneuverability of the target, tracking error of the spindle system, visual axis jitter caused by wind resistance torque, stability of the foundation, stiffness of the frame and turbulence of the atmosphere, fine tracking system needs higher tracking requirements. In recent years, some methods are widely used in high-precision tracking system [5]–[7]. Nevertheless, external disturbance and hysteresis phenomenon are the two main factors that affect the system accuracy. Therefore, these two drawbacks must be eliminated for achieving high-precision control.

The active disturbance rejection control (ADRC) was first put forward by Han [8], which is efficient for estimating and compensating the uncertainties. Traditional ADRC mainly includes three parts: a

tracking differentiator (TD), an extended state observer (ESO) and a nonlinear state error feedback (NLSEF). So ADRC strategy was developed to handle various uncertainties in some applications [9]–[12]. The key points of ADRC are to use ESO to estimate the disturbance and design the control law to ensure the stability of the system. In [13], a parameterized linear ADRC (LADRC) was first proposed by Gao, which makes the controller design and tuning easier and more efficient. In [14], an active disturbance rejection adaptive control scheme via full state feedback for motion control of hydraulic servo systems subjected to both parametric uncertainties and uncertain nonlinearities. In [15], a modified ADRC combined with a project gradient estimator was proposed. The ADRC has made great progress in recent years.

Hysteresis is unavoidable in piezoelectric actuation devices, and it has a certain effect on the accuracy of the system. Some hysteresis models were built to compensate for this phenomenon, such as Preisach Model, Duhem Model, Maxwell Model and Bouc–Wen Model [16]. Generally speaking, models can not completely describe the hysteresis phenomenon, so this method of compensating hysteresis has some disadvantages. This method of compensation is based on previously established models, so some model-free methods developed in recent years [17].

Iterative learning control (ILC) is based on the design of input and output information and it does not require an exact model. ILC updates the next control output on the basis of the previous control output and the error information. In addition, ILC does not need the disturbance signals be known or measured, only that these signals repeat from iteration to iteration. Due to this feature, ILC is widely utilized in industrial robots [18], rapid thermal processing [19], cold rolling mills [20], and induction motors [21]. ILC is also applied to some systems that do not need identical repetition. In [22], ILC serves as a training mechanism for open loop control. In [23], researchers use ILC to develop high peak power microwave tubes. ILC is also used to obtain the aerodynamic drag coefficient for a projectile [24]. Especially in [25] and [26], ILC has been successfully employed to restrain the influence of the hysteresis in piezoelectric actuation devices.

In this paper, a new control structure that contains improved active disturbance rejection control (ADRC) and iterative learning control (ILC) is adopted to compensate the above disturbance. This strategy combines the advantages of the two methods, which can not only eliminate the external disturbance but also eliminate the hysteresis effect. Unlike the traditional ADRC, this method adopts sliding mode control (SMC) instead of NLSEF and adopts forgetting polynomial ILC, so as to achieve fast convergence and good robustness. Compared to the traditional FSM control system, the proposed ADRC-ILC strategy has the following properties: 1) applicable to estimate unknown disturbances; 2) hysteresis model is not required anymore; 3) a new ADRC combines with ILC control structure. The effectiveness of the control algorithm is verified by simulation and experiments.

The rest organization of this paper is as follows. In the Section 2, the mathematical model of FSM is set up. In the Section 3, the ADRC method and ILC method are designed with the convergence analysis of two methods respectively. In the Section 4, the theoretical simulation and the experimental results are introduced. In the Section 5, this part draws a conclusion and points out the direction of future discussion.

2. The Dynamic Mathematical Model of FSM

The simplified structure of FSM is shown in Fig. 1. Piezoelectric actuators (PEAs) are the primary parts in FSM system which can drive FSM with ± 1 mrad via flexible bearing. In addition, the high resolution charge-coupled device (CCD) is used to detect spot position. Due to the two axes are independent of each other, and the servo design method is alike, so the article chooses the azimuth axis as the research object.

According to the principle of piezoelectric driven mirror, the FSM position open-loop can be described by the second-order mechanical resonance model [27]. More specifically, the following transfer function can express the model of PEA plant model:

$$G_p(s) = \frac{x(s)}{u(s)} = \frac{k\omega_n^2}{s^2 + 2\zeta\omega_n s + \omega_n^2} \tag{1}$$

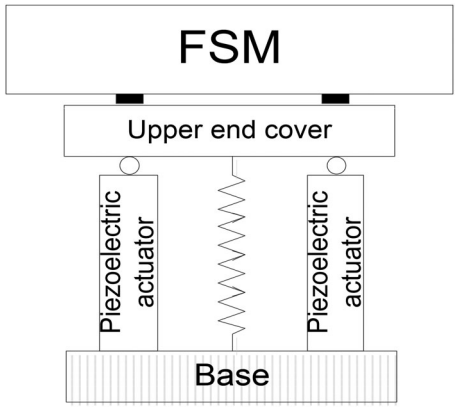

Fig. 1. Simplified structure of FSM.

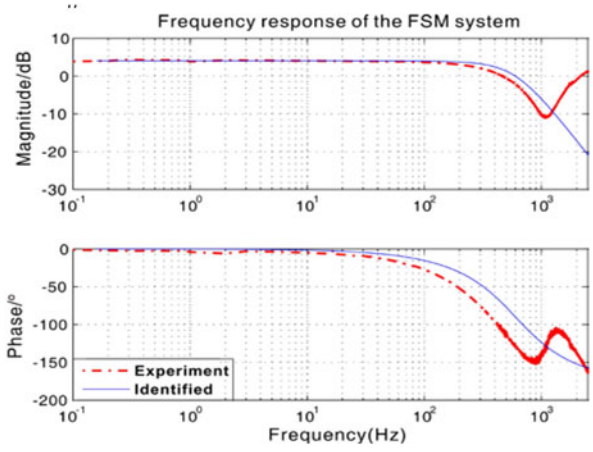

Fig. 2. Experimental frequency response of the FSM system.

Where x and u are the position output and control input, respectively. The parameters k, ω_n and ζ are the plant gain, resonant frequency and damping ratio, respectively. These unknown parameters can be identified from experimental frequency response data. FSM open-loop frequency response results are shown in Fig. 2. To carry out the control design for simplicity, the transfer function of the system is represented as follows:

$$\ddot{x}(t) + a_1\dot{x}(t) + a_0x(t) = bu(t) + d(t, x) \tag{2}$$

Where $a_0 = \omega_n^2$, $a_1 = 2\zeta\omega_n$, $b = k\omega_n^2$, and $d(t)$ denotes the lumped external disturbances.

3. The Control Design for FSM System

3.1 Improved Active Disturbance Rejection Controller Design

Traditional ADRC mainly includes three parts: a tracking differentiator (TD), an extended state observer (ESO) and a nonlinear state error feedback (NLSEF). On this basis, an enhanced ADRC that using sliding mode control (SMC) instead of the traditional NLSEF method is proposed to attenuate the influence of the unknown and unmolded parts.

3.1.1 The Tracking differentiator: In the improved ADRC, the TD is used as a transient process. TD can avoid the delay effect of obtaining a differential signal from the traditional inertial element.

The expression of TD is designed as follows:

$$\begin{cases} \text{fh} = \text{fhan}\left(v_1 - y_d, v_2, r, h\right) \\ \dot{v}_1 = v_2 \\ \dot{v}_2 = \text{fh} \end{cases} \tag{3}$$

Where y_d is ideal input signal of the system, v_1 is the tracking signal of y_d, v_2 is the differentiation of y_d when v_1 tracks y_d. fhan(v_1, v_2, r, h) is an optimal control synthesis function that can be given as:

$$\text{fhan}\left(v_1, v_2, r, h\right) = -\begin{cases} r\text{sgn}\left(\alpha\right), & |\alpha| > \delta \\ r\frac{\alpha}{\delta}, & |\alpha| \le \delta \end{cases} \tag{4}$$

Where

$$\alpha = \begin{cases} v_2 + \frac{\alpha_0 - \delta}{2}\text{sgn}\left(y\right), & |y| > \delta_0 \\ v_2 + \frac{y}{h}, & |y| \le \delta_0 \end{cases} \tag{5}$$

$$\begin{cases} \delta = rh \\ \delta_0 = \delta h \\ y = v_1 + hv_2 \\ \alpha_0 = \sqrt{\delta^2 + 8r\left|y\right|} \end{cases} \tag{6}$$

Where r and h are fast factor and filter factor, respectively. Besides, the greater the value of r, the faster the tracking speed and the larger the value of h, the better the filtering effect. However, excessive values can cause high-frequency tremors. We can select the appropriate parameters according to the performance requirements of the actual system.

3.1.2 The Extended State Observer: The ESO estimates the disturbance as an extra state, hence it can compensate the disturbance. According to the above analysis, system state space representation can be described from (2) as follows:

$$\begin{cases} \dot{x}_1(t) = x_2(t) \\ \dot{x}_2(t) = -a_0x_1(t) - a_1x_2(t) + bu(t) + d(t, x) \\ y(t) = x_1(t) \end{cases} \tag{7}$$

Here, let $f_0(x_1(t), x_2(t)) = -a_0x_1(t) - a_1x_2(t)$, which denotes the modeled part and $d(t, x)$ denotes the all unknown part. Before presenting the proposed ESO scheme, the following assumption is first addressed

Assumption 1: The disturbance $d(t, x)$ is bounded, continuous and differential, $|d(t, x)| \le D\,, \forall t \in (0, \infty)$, where D is a unknown constant, and let $p\left(t\right) = -\frac{dd(t,x)}{dt}$. Moreover, $p(t)$ is bounded such that $|p\left(t\right)| \le \gamma, \forall t \in (0, \infty)$, where γ is a positive constant.

Therefore, we define the $d(t, x)$ as a state x_3 of the system. So the state space representation can be rewrited as follows:

$$\begin{cases} \dot{x}_1(t) = x_2(t) \\ \dot{x}_2(t) = f_0(x_1(t), x_2(t)) + bu(t) + d(t, x) \\ \dot{x}_3(t) = -p\left(t\right) \\ y(t) = x_1(t) \end{cases} \tag{8}$$

The third-order equation of the ESO is as follows:

$$\begin{cases} e_1 = z_1 - y \\ \dot{z}_1 = z_2 - \beta_{01}e_1 \\ \dot{z}_2 = z_3 - \beta_{02}e_1 + f_0(z_1, z_2) + bu \\ \dot{z}_3 = -\beta_{03}e_1 \end{cases} \tag{9}$$

Where z_i is the estimated value of x_i, $i = 1, 2, 3$, e_1 is the observer error, β_{01}, β_{02}, and β_{03} are the observer parameters. Control law can be designed as:

$$u = \frac{(u_0 - z_3)}{b} \tag{10}$$

Therefore, the following observation error matrix is obtained

$$\dot{E} = A\,E + Bp \tag{11}$$

Where,

$$E = [e_1\ e_2\ e_3]^{\mathrm{T}},\ e_2 = z_2 - x_2,\ e_3 = z_3 - x_3,\ A = \begin{bmatrix} -\beta_{01} & 1 & 0 \\ -\beta_{02} & 0 & 1 \\ -\beta_{03} & 0 & 0 \end{bmatrix},\ B = [\,0\,0\,1\,]^{\mathrm{T}}$$

It is notable that if ESO is Bounded-Input Bounded-Output (BIBO) stable, the eigenvalues of matrix A are to the left of the S-plane, so that the matrix A is Hurwitzs. Eigenvalue equation of matrix A is as follows:

$$\lambda^3 + \beta_{01}\lambda^2 + \beta_{02}\lambda + \beta_{03} = (\lambda + \omega_0)^3 \tag{12}$$

Therefore, the parameters β_{01}, β_{02} and β_{03} can be selected as:

$$\beta_{01} = 3\omega_0,\ \beta_{02} = 3\omega_0^2,\ \beta_{03} = \omega_0^3 \tag{13}$$

According to the above analysis, we can know that only one positive parameter ω_0 need to be adjusted to complete the design of ESO. This method simplifies the design process of ESO.

3.1.3 The Design of Sliding Mode Control: Compared with traditional ADRC, the controller mentioned in this paper adopts the sliding mode control (SMC), by doing this, the NLSEF is replaced, which reduces the impact of shocks and then improves the stability of tracking process.

Before designing the controller, we first define a few variables with the previous analysis

$$e = v_1 - z_1 \approx y_d - x_1,\ \dot{e} = v_2 - z_2 \approx \dot{y}_d - x_2,\ \ddot{e} = \ddot{y}_d - \dot{x}_2 \tag{14}$$

Where e, $\dot{e}$, and $\ddot{e}$ represent the position error, the velocity error, and the acceleration error, respectively.

The sliding mode surface can be defined as follows to ensure $e = 0$.

$$s = ce + \dot{e} \tag{15}$$

Where the coefficient is $c > 0$, the derivative of the sliding surface along with the system given in (8), will be calculated as follows:

$$\begin{aligned} \dot{s} &= c\dot{e} + \ddot{e} \\ &= c\dot{e} + \ddot{y}_d + a_0 x_1 + a_1 x_2 - bu - d \end{aligned} \tag{16}$$

In order to obtain fast response, robustness and effective elimination of sliding mode chattering, the reaching law is designed by the following function

$$\dot{s} = -\lambda_1 s - \mu_1 s^{q_1/p_1} \tag{17}$$

Where λ_1 and μ_1 are positive constants, q_1 and p_1 are positive odd integers, which should satisfy $0 < q_1/p_1 < 1$. Considering the two mentioned equations (16) and (17), we get the control law is given as follows:

$$u_0 = \frac{1}{b}\left(c\dot{e} + \ddot{y}_d + a_0 x_1 + a_1 x_2 + \lambda_1 s + \mu_1 s^{q_1/p_1} - d\right) \tag{18}$$

Because d cannot be fully compensated, we further modify the control law as follows:

$$u_0 = \frac{1}{b}\left(c\dot{e} + \ddot{y}_d + a_0 x_1 + a_1 x_2 + \lambda_1 s + \mu_1 s^{q_1/p_1} + \mathrm{sgn}\,(s)\,\hat{D}\right) \tag{19}$$

Where $\hat{D}$ is the estimated value of D, and we define $\tilde{D} = D - \hat{D}$ is unknown parameter estimate errors.

Theorem 1: Considering the dynamic mathematical model of system (8) with the sliding mode control law designed in (19) and with the adaptive laws

$$\dot{\hat{D}} = \gamma_1 |s| \tag{20}$$

There exist parameters $c > 0$, $\lambda_1 > 0$, $\mu_1 > 0$, $\gamma_1 > 0$, the odd integers q_1, p_1 and $0 < q_1/p_1 < 1$ can guarantee that the system output tracking error will asymptotically converge to zero.

Proof: Considering the Lyapunov function

$$V = \frac{1}{2}s^2 + \frac{1}{2\gamma_1}\tilde{D}^2 \tag{21}$$

The derivative of the function (21) is

$$\begin{aligned}\dot{V} &= s\dot{s} + \frac{1}{\gamma_1}\tilde{D}\dot{\tilde{D}} \\ &= -\lambda_1 s^2 - \mu_1 s^{\frac{p_1+q_1}{p_1}} - \frac{1}{\gamma_1}\tilde{D}\dot{\hat{D}} - ds - \hat{D}|s| \\ &= -\lambda_1 s^2 - \mu_1 s^{\frac{p_1+q_1}{p_1}} - \frac{1}{\gamma_1}\tilde{D}\dot{\hat{D}} - ds - D|s| + D|s| - \hat{D}|s|\end{aligned} \tag{22}$$

Note that $|d(t, x)| \le D$, so we get $ds + D|s| \ge 0$

$$\begin{aligned}\dot{V} &\le -\lambda_1 s^2 - \mu_1 s^{\frac{p_1+q_1}{p_1}} - \frac{1}{\gamma_1}\tilde{D}\dot{\hat{D}} + D|s| - \hat{D}|s| \\ &\le -\lambda_1 s^2 - \mu_1 s^{\frac{p_1+q_1}{p_1}} - \frac{1}{\gamma_1}\tilde{D}\dot{\hat{D}} + \tilde{D}|s| \\ &\le -\lambda_1 s^2 - \mu_1 s^{\frac{p_1+q_1}{p_1}} + \tilde{D}\left(|s| - \frac{1}{\gamma_1}\dot{\hat{D}}\right)\end{aligned} \tag{23}$$

Substituting the adaptive laws (20) into (23), $\dot{V}$ can be written as:

$$\dot{V} \le -\lambda_1 s^2 - \mu_1 s^{\frac{p_1+q_1}{p_1}} \tag{24}$$

Thus, we have

$$\dot{V} \le 0 \tag{25}$$

Therefore, this result explains that the designed controller is stable and the output tracking error will converge to zero in a limited time. The proof of theorem (1) is completed.

3.2 Iterative Learning Controller Design

As the piezoelectric actuators will appear hysteresis effect. The modeling compensation method has the disadvantage of incapability of accurately describing the hysteresis phenomenon, so this paper chooses a model-free compensation strategy. This article adopts an iterative learning method with a forgetting factor, which makes the impact on the initial state becomes smaller and smaller as the number of iterations increases and enhances the system's ability to suppress initial errors and changes in system parameters. The control structure of the algorithm is shown in Fig. 3.

According to (1), the plant model can be described as follows:

$$\begin{cases}\dot{x}_k = A x_k + B u_k \\ y_k = c x_k\end{cases} \tag{26}$$

Where $A = \begin{bmatrix} 0 & 1 \\ -a_0 & -a_1 \end{bmatrix}$, $B = \begin{bmatrix} 0 \\ 1 \end{bmatrix}$, c = [0 1] and k is the numbers of iterations.

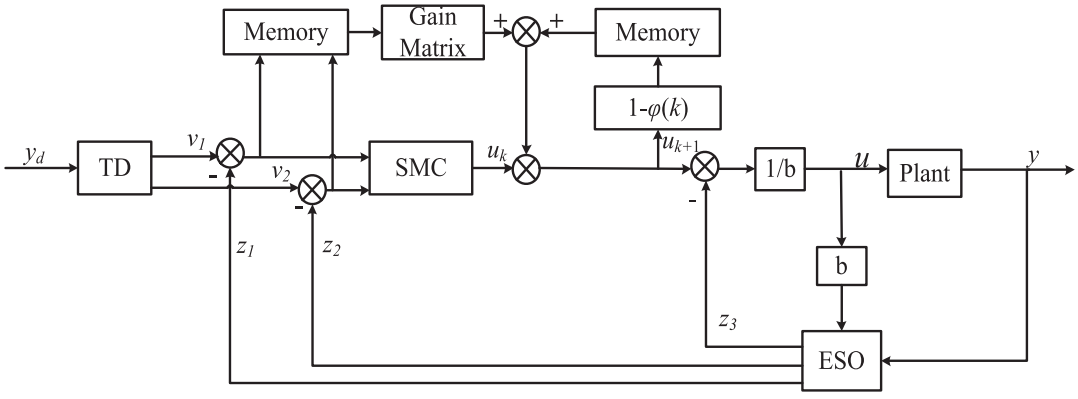

Fig. 3. Structure of the improved ADRC-ILC control.

Assumption 2: There is an ideal input signal $u_d(t)$ that enables the system to track the desired output trajectory $y_d(t)$ on a finite time interval [0, T].

$$\begin{cases} \dot{x}_d = A x_d + B u_d \\ y_d = c x_d \end{cases} \tag{27}$$

Assumption 3: The FSM system initial conditions to meet:

$$x_k(0) = x_d(0)\, k = 0, 1, 2, 3 \ldots \tag{28}$$

In order to make the iterative learning sequence $u_k(t)$ uniformly converge to the ideal control input $u_d(t)$, we must find a suitable learning law so that the system output $y_k(t)$ can track the ideal output $y_d(t)$, $\forall t \in [0, T]$. The purpose of introducing a forgetting factor $\varphi(k)$ is to give the original output and the new output different weights so that the algorithm has the ability to respond quickly to changes in the input process characteristics. In this work, we select the following ILC scheme:

$$u_{k+1}(t) = (1 - \varphi(k))\, u_k(t) + \varphi(k) u_0(t) + P e_k(t) + \Gamma \dot{e}_k(t) \tag{29}$$

Where $\varphi(k)$ is forgetting polynomial factor, $\varphi(k) \in [0, 1]$, P and Γ are gain matrix, $P \in \mathbf{R}^{m \times q}$, $\Gamma \in \mathbf{R}^{m \times q}$, $e_k(t)$ is the error between the kth iterative output and the ideal output.

3.2.1 Convergence Analysis of ILC Output Tracking Error:

Theorem 2: If the system satisfies the assumptions 2 and assumptions 3, then when the system meets the following conditions (30) and (31), then the position tracking error $e_k(t)$ converges to zero asymptotically.

$$\left\| (1 - r(k)) I - \Gamma C B \right\| \leq \delta < 1 \tag{30}$$

$$\lim_{k \to \infty} r(k) = 0 \tag{31}$$

Proof: To prove that the algorithm is convergent, combined with the above analysis, we know $e_k(t) = y_d(t) - y_k(t)$. Taking into account equations (26) and (27) and bringing the solution of the state variable $x_d(t)$ and $x_k(t)$ inhomogeneous equation into it, we can get the following equation:

$$\begin{aligned} e_{k+1}(t) &= y_d(t) - y_{k+1}(t) = c[x_d(t) - x_{k+1}(t)] \\ &= c e^{At}[x_d(0) - x_k(0)] + \int_0^t c e^{A(t-\tau)} B(u_d(\tau) - u_k(\tau)) d\tau \end{aligned} \tag{32}$$

To prove the convergence of the above formula and consider (29)

$$\begin{aligned} u_d(t) - u_{k+1}(t) &= u_d(t) - (1 - r(k))\, u_k(t) - r(k)\, u_0(t) - P e_k(t) - \Gamma \dot{e}_k(t) \\ &= (1 - r(k))\,[u_d(t) - u_k(t)] + r(k)\,[u_d(t) - u_0(t)] \\ &\quad - Pc\,[x_d(t) - x_k(t)] - \Gamma A c\,[x_d(t) - x_k(t)] - \Gamma B c\,[u_d(t) - u_k(t)] \\ &= [(1 - r(k))\, I - \Gamma B c]\,[u_d(t) - u_k(t)] - (Pc + \Gamma A c)\, e^{At} \\ &\quad \times [x_d(0) - x_k(0)] - (Pc + \Gamma A c) \int_0^t e^{A(t-\tau)} B\,[u_d(t) - u_k(t)]\, d\tau \end{aligned} \tag{33}$$

Taking the norm $\| \bullet \|$ simultaneously on both sides of the equation (33)

$$\begin{aligned} \|u_d(t) - u_{k+1}(t)\| &\le \|(1 - r(k))\, I - \Gamma B c\| \cdot \|u_d(t) - u_k(t)\| + e^{At}\, \|Pc + \Gamma A c\| \\ &\quad \times \|x_d(0) - x_k(0)\| + \|Pc + \Gamma A c\| \cdot \int_0^t e^{A(t-\tau)} B\, \|u_d(\tau) - u_k(\tau)\|\, d\tau \end{aligned} \tag{34}$$

Multiplying by a positive function $e^{-\lambda t}$, $t \in [0, \mathrm{T}]$, and we get

$$\begin{aligned} \|u_d(t) - u_{k+1}(t)\|\, e^{-\lambda t} &\le \|(1 - r(k))\, I - \Gamma B c\| \cdot \|u_d(t) - u_k(t)\|\, e^{-\lambda t} + e^{(\|A\| - \lambda)t}\, \|Pc + \Gamma A c\| \\ &\quad \times \|x_d(0) - x_k(0)\| + \|Pc + \Gamma A c\| \cdot \int_0^t e^{(\|A\| - \lambda)(t-\tau)} e^{-\lambda \tau} B\, \|u_d(\tau) - u_k(\tau)\|\, d\tau \\ &\le \|(1 - r(k))\, I - \Gamma B c\| \cdot \|u_d(t) - u_k(t)\|\, e^{-\lambda t} + e^{(\|A\| - \lambda)t}\, \|Pc + \Gamma A c\| \\ &\quad \times \|x_d(0) - x_k(0)\| + \frac{\|Pc + \Gamma A c\| \cdot \|B\| \cdot \left(1 - e^{(\|A\| - \lambda)t}\right)}{\lambda - \|A\|} \\ &\quad \cdot \|u_d(t) - u_k(t)\|\, e^{-\lambda t} \end{aligned} \tag{35}$$

We refer to the λ norm for a function $h : [0, T] \to \mathrm{R}^k$ by [28]:

$$\|h(\bullet)\|_\lambda \triangleq \sup_{t \in [0, \mathrm{T}]} e^{-\lambda t}\, \|h(t)\| \tag{36}$$

Taking the λ norm on both sides of (35), we have

$$\begin{aligned} \|u_d(t) - u_{k+1}(t)\|_\lambda &\le \left\| [(1 - r(k))\, I - \Gamma B c] + \frac{\|Pc + \Gamma A c\| \cdot \|B\| \cdot \left(1 - e^{(\|A\| - \lambda)t}\right)}{\lambda - \|A\|} \right\| \\ &\quad \cdot \|u_d(t) - u_k(t)\|_\lambda + e^{(\|A\| - \lambda)t}\, \|Pc + \Gamma A c\| \cdot \|x_d(0) - x_k(0)\| \end{aligned} \tag{37}$$

Moreover, based on the previous formula (30), we can find a λ that is much greater than $\|A\|$ which makes

$$\sigma = \left\| [(1 - r(k))\, I - \Gamma B c] + \frac{\|Pc + \Gamma A c\| \cdot \|B\| \cdot \left(1 - e^{(\|A\| - \lambda)t}\right)}{\lambda - \|A\|} \right\| < 1$$

Then, for $\sigma < 1$ we have

$$\|u_d(t) - u_{k+1}(t)\|_\lambda \le \left(\frac{\|Pc + \Gamma A c\|}{1 - \sigma} \right) \cdot \|x_d(0) - x_k(0)\| \tag{38}$$

Remark 1: The λ norm of $\|u_d(t) - u_{k+1}(t)\|$ regards $(\frac{\|Pc+\Gamma A c\|}{1-\sigma}) \cdot \|x_d(0) - x_k(0)\|$ as the radius of convergence. In addition, the value of the convergence radius depends on the initial conditions $(x_d(0) - x_k(0))$. And if the system satisfies the hypothetical condition (28), the k*th* iteration of the input $u_k(t)$ converges to the ideal control input $u_d(t)$.

Next, taking the λ norm $\| \bullet \|_\lambda$ on both sides of (32)

$$\begin{aligned}\left\| e_{k+1}(t) \right\|_\lambda &= ce^{At} \left\| [x_d(0) - x_{k+1}(0)] + \int_0^t ce^{A(t-\tau)} B(u_d(\tau) - u_{k+1}(\tau)) d\tau \right\|_\lambda \\ &\leq e^{(\|A\|-\lambda)t} \|c\| \cdot \left\| x_d(0) - x_{k+1}(0) \right\| + \frac{\|c\| \cdot \|B\| \cdot \left(1 - e^{(\|A\|-\lambda)t}\right)}{\lambda - \|A\|} \cdot \left\| u_d(t) - u_{k+1}(t) \right\|_\lambda \end{aligned} \tag{39}$$

Substituting (38) into (39), a necessary algebra operation leads to

$$\begin{aligned}\left\| e_{k+1}(t) \right\|_\lambda &\leq e^{(\|A\|-\lambda)t} \|c\| \cdot \left\| x_d(0) - x_{k+1}(0) \right\| \\ &+ \frac{\|c\| \cdot \|B\| \cdot \left(1 - e^{(\|A\|-\lambda)t}\right)}{\lambda - \|A\|} \cdot \left(\frac{\|Pc + \Gamma A\, c\|}{1 - \sigma} \right) \left\| x_d(0) - x_k(0) \right\| \end{aligned} \tag{40}$$

In consideration of (28), we can know that

$$\lim_{k \to \infty} \| e_{k+1}(t) \|_\lambda = 0 \tag{41}$$

With the above description, we can see that if this approach is used and the mentioned conditions are met, the control input $u_k(t)$ converges to the ideal control input $u_d(t)$ and the error $e_k(t)$ converges to zero, further illustrating that the output $y_k(t)$ can track the ideal output curve $y_d(t)$.

4. Simulation and Experimental Results

4.1 Simulation Study

In order to validate the effectiveness of proposed improved ADRC controller, we carried out the simulation in Matlab/Simulink environment. First, the simulation is performed to verify the features of proposed control strategy. Combined with reference [27] and open loop frequency characteristic curves showed in Fig. 2, we select a second-order mechanical model as our controlled object. A sinusoid $y_d(t) = \sin(t)$ μm is regarded as a desired input trajectory for reference. In order to better explain the improved ADRC controller can effectively suppress the internal disturbance and external random interference, so we chose $d(\mathrm{t}, \mathrm{x}) = -25x_2 + 33\sin(\pi t) + \mathrm{N(t)}$ as disturbance signal where N(t) represents a random disturbance signal with maximum amplitude of 5. The former formula $-25x_2$ expresses internal disturbance, and the latter expression $33\sin(\pi \mathrm{t}) + \mathrm{N(t)}$ expresses external random disturbance. The tracking output curve of each control strategy is shown in the Fig. 4. We can see from the system tracking curve that the trajectory of the improved ADRC is closer to the reference, especially the error at the peak value 0.05 μm is much smaller than the traditional ADRC peak error 0.9 μm. In addition, when the system is steadily stabilized, the error of the improved algorithm 0.005 μm is also smaller than the traditional ADRC value 0.015 μm. The reason is that SMC has a better ability to resist disturbance than the traditional NLSEF. In summary, we can see that the improved algorithm has better performance from tracking trajectory and error curve. Therefore, the improved ADRC controller is effective and we will continue to verify its performance in the actual experiment.

4.2 Experimental Setup

The experimental setup of the FSM tracking loop system is shown in Fig. 5(a). There are two FSMs used to accomplish the entire work, one is used to simulate external disturbances, the other is used to receive control signal from DSP for tracking. The FSM system control loop is depicted in Fig. 5(b). The platform consists of the following devices: 1) FSMs (model: S-330, from Physik Instrumente) with the diameter of 25.4 mm; 2) Laser (PGL-V-H-635) providing the signal light with wavelength of 635 nm; 3) Collimator lens with the diameter of 55 mm and the focal length of 550 mm; 4) Cassegrain Telescope (from Schmidt) with the diameter of 150 mm and the total focal length with objective lens of 1500 mm; 5) Camera(model: MC3086, from MIKROTRON) with the pixel size of 8 $*$ 8 μm.

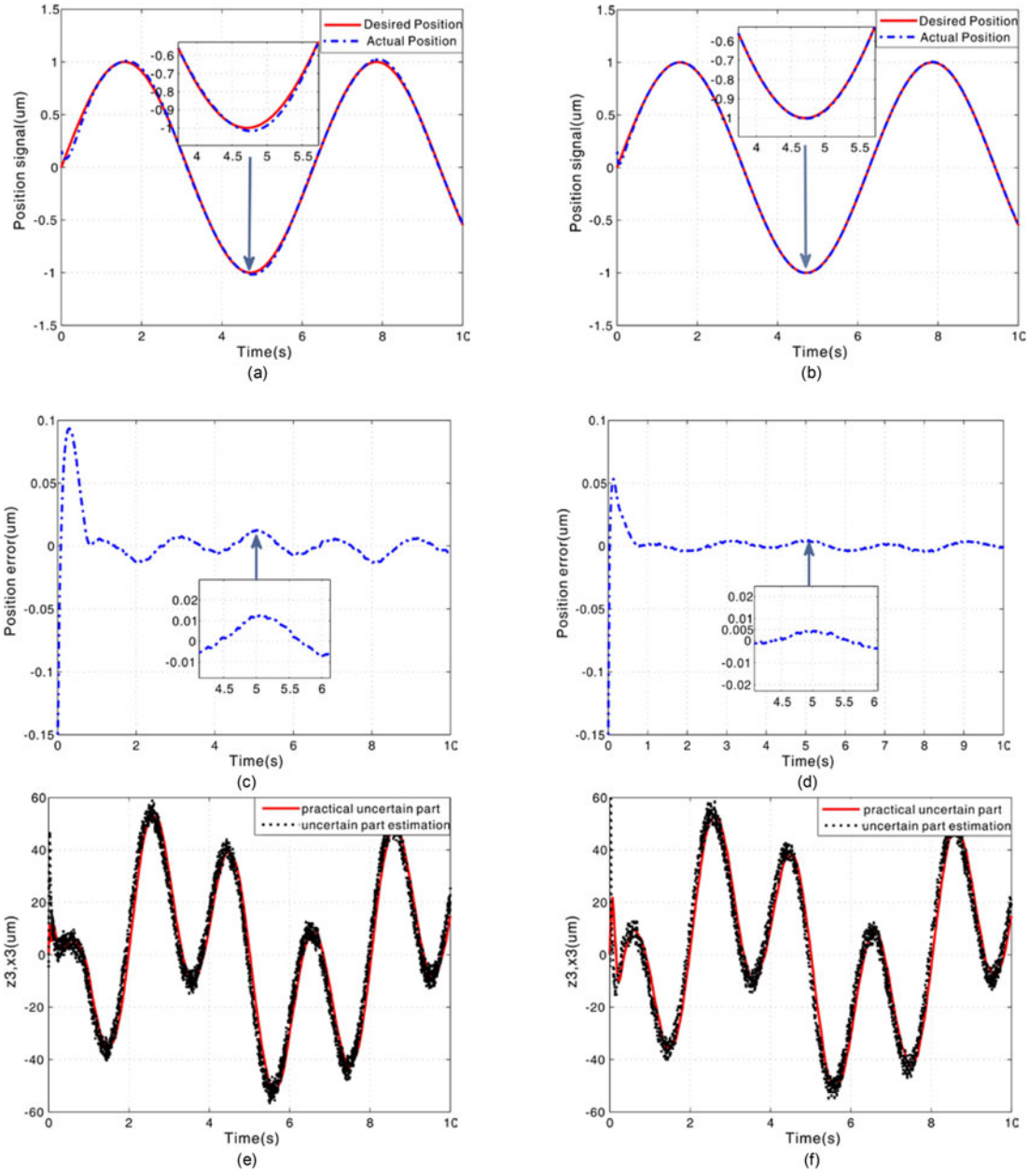

Fig. 4. Simulation results of ADRC and improved ADRC. (a) Reference and actual position trajectories of ADRC. (b) Reference and actual position trajectories of improved ADRC. (c) Tracking error of ADRC. (d) Tracking error of improved ADRC. (e) ESO output of ADRC. (f) ESO output of improved ADRC.

First, the signal light beam produced by a laser reaches the disturbance FSM after being collimated and expanded. The disturbance FSM is used to simulate jitter of the target. Then the controlled FSM will correct the perturbed beam. Finally, the corrected beam will be imaged by the camera after shrinking through the telescope. The disturbance FSM is governed by Physik Instrumente (PI) driver to simulate disturbance. The other FSM is controlled by DSP-TMS320F28335 with sampling frequency 1 kHz that inhibits the disturbance. The proposed control algorithm is achieved by using a C-program in DSP. The communication between camera and DSP is done by Field Programmable Gate Array (FPGA-EP4CE30F23C6N).

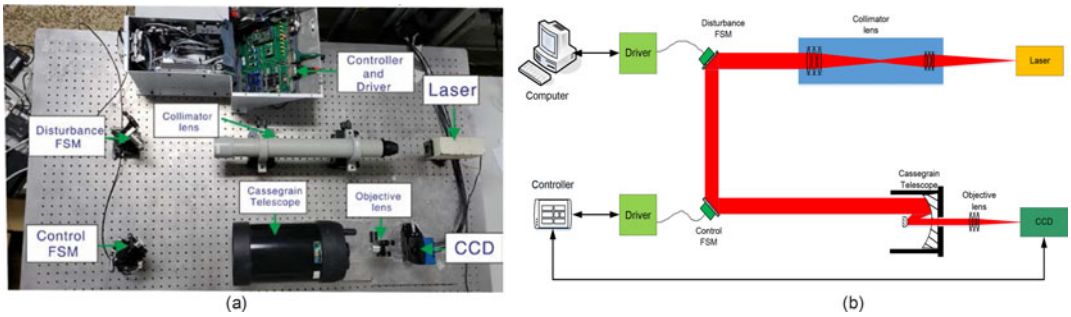

Fig. 5. Experimental setup. (a) Prototype of experimental platform. (b) Schematic diagram of tracking system.

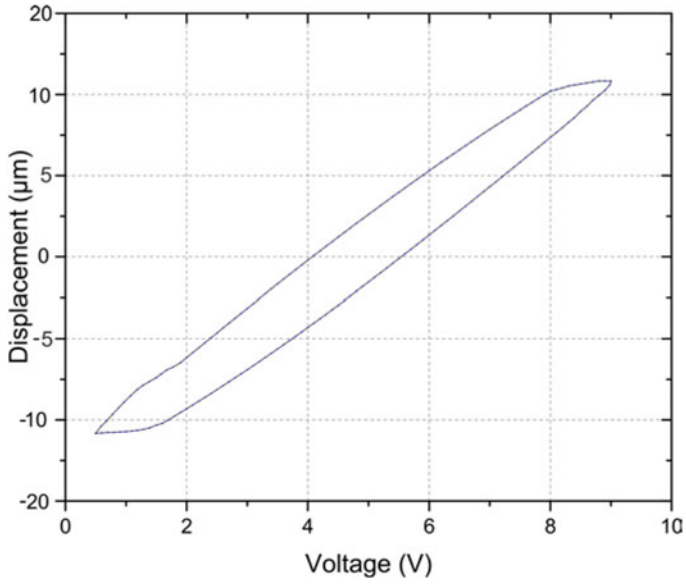

Fig. 6. Hysteresis effect in the piezoeletric actuators.

4.3 Hysteresis Characterization

In this article, the hysteresis effect of the FSM high precision positioning system which is driven by the piezoelectric actuators is inevitable. Fig. 6 shows the open-loop hysteresis effect of piezoelectric actuator with input frequency 10 Hz before carrying out the improved control strategy. As shown in Fig. 6, we know that the forward trajectory of the actuators does not coincide with the reverse trajectory, and the hysteresis phenomenon does exist in the actuators. Obviously, the piezoelectric actuator has a position range around ± 10 μm. Generally speaking, the greater frequency and amplitude of the input signal, the more apparent the hysteresis is. Therefore, in order to achieve accurate motion control at high working frequency in a large input range, hysteresis compensation is essential. The next experiment will compensate for this hysteresis loop.

In order to reduce the error of the system caused by hysteresis and improve the FSM precision tracking system accuracy, ILC is used to compensate hysteresis. Point-to-point experiments on a single FSM are carried out to verify this method. We let the FSM take a positively increasing ramp signal and then decrease it in the opposite direction along the original path. Fig. 7 is the result of system with and without the ILC method to compensate. Comparing the two curves, we can see that the ILC method can make the linearity of the output curve better. The width of the hysteresis loop obtained by the ILC method is smaller than that without ILC compensation. The experimental results further show that the recommended ILC method is effective for compensating hysteresis.

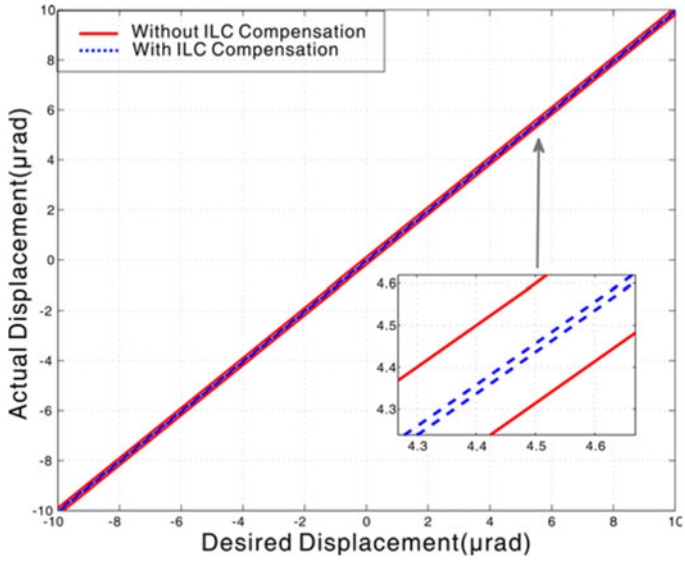

Fig. 7. Hysteresis compensation diagram of ILC and without ILC.

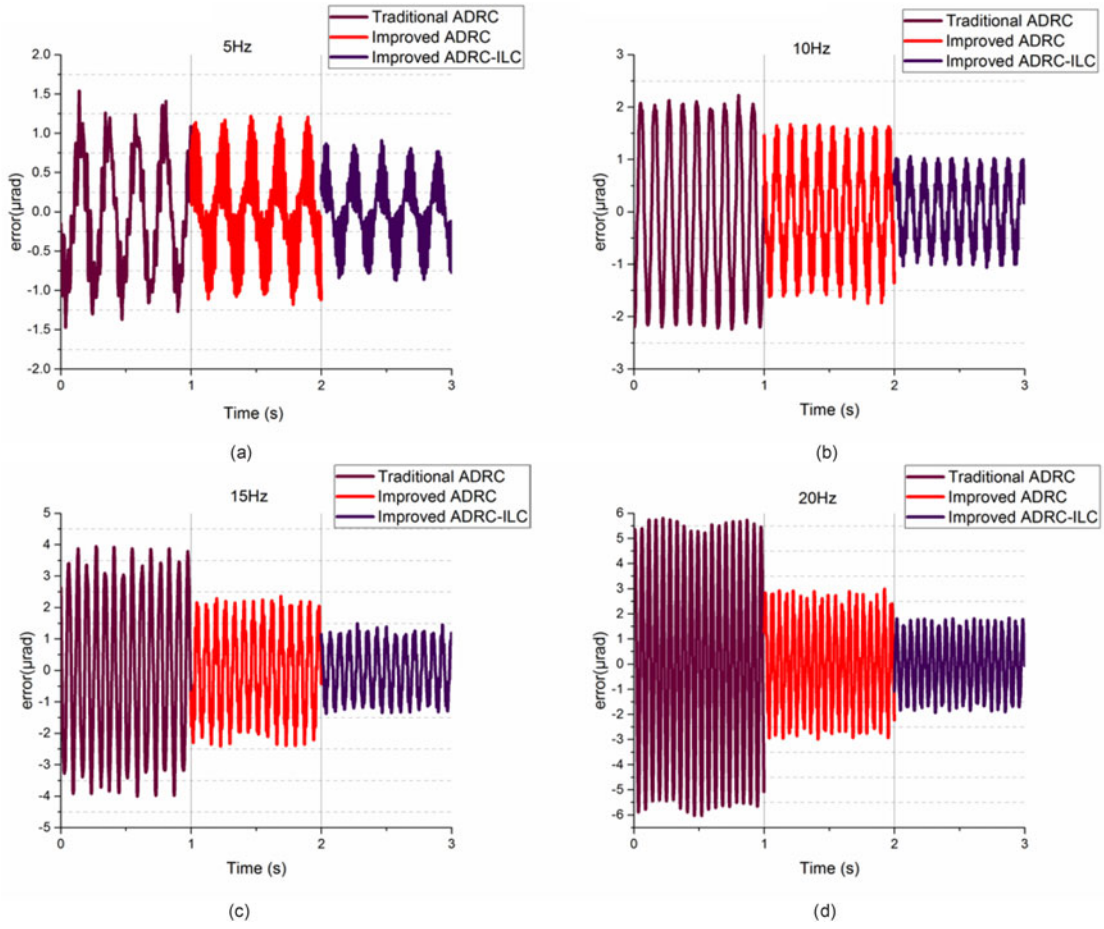

Fig. 8. Experimental diagrams of tracking error. (a) Tracking error of 5 Hz. (b) Tracking error of 10 Hz. (c) Tracking error of 15 Hz. (d) Tracking error of 20 Hz.

TABLE 1
Experimental Results of the Three Controllers

Control strategy	Performance(μrad)	5Hz-sinusoid	10 Hz-sinusoid	15 Hz-sinusoid	20 Hz-sinusoid
Traditional ADRC	RMSE	0.75	1.50	2.45	3.96
	|Max|	1.54	2.24	3.95	6.03
Improved ADRC	RMSE	0.57	0.91	1.31	1.73
	|Max|	1.22	1.75	2.41	2.99
Improved ADRC-ILC	RMSE	0.37	0.60	0.84	1.14
	|Max|	0.91	1.06	1.50	1.93

4.4 Experimental Results

The simulation shows the good performance of the controller. On this basis, we carried out experiments to verify the performance of the FSM system. Through the open-loop frequency response results showed in Fig. 2, we can identify the controlled system parameters $a_0 = \omega_n^2 = 1.42 \times 10^7$, $a_1 = 2\zeta\omega_n = 6.03 \times 10^3$, $b = k\omega_n^2 = 2.26 \times 10^7$. The parameters of the improved ADRC are selected as $r = 50$, $h = 0.01$, $\delta = rh = 0.5$, $\delta_0 = \delta h = 0.005$, $\omega_0 = 10$, $\beta_{01} = 30$, $\beta_{02} = 300$, $\beta_{03} = 1000$, c $= 100$, $\mu_1 = 300$, $\lambda_1 = 200$, $p_1 = 7$, $q_1 =, 5$ and the parameters of ILC are chosen as $\varphi(k) = 1/k^3$, $p = 1$, $\Gamma = 0.5$. According to a large number of practical engineering experience, disturbance signals are generally low-frequency signals. We conducted perturbation inhibition experiments of 5 Hz-50 μrad, 10 Hz-50 μrad, 15 Hz-50 μrad, and 20 Hz-50 μrad as amplitude sinusoidal disturbances, respectively. The experimental results are shown in Fig. 8. We can see that the disturbance rejection effect of improved ADRC is better than that of traditional ADRC and ILC can reduce the error further. The reason is that the system perturbation is further compensated by subtracting the nonlinear perturbation with the ILC algorithm. An easy comparison for the maximum error and root mean square error (RMSE) under tests are listed in Table 1.

Compared with the traditional ADRC at low frequency like 5 Hz, the error of improved ADRC-ILC is 0.91 μrad. We can get a general conclusion from the calculation of data in the Table 1, the improved ADRC-ILC controller reduces the maximum error and RSME by 41% and 51%, respectively. In addition, compared with the improved ADRC without ILC scheme, the improved ADRC-ILC controller further reduces the maximum error and RSME by 25% and 35%, respectively. And at medium-high frequency, the improved ADRC-ILC controller also shows the good capability, which reduces the RSME by 60% and 34%, respectively. Therefore, the experimental results indicate that the improved ADRC-ILC control scheme has better performance over traditional ADRC and improved ADRC schemes in tracking precision.

5. Conclusion

In this paper, we proposed a new improved ADRC with ILC structure for fine tracking system of FSO communications and proved the convergence of the algorithm. In addition, we have done some simulations and experiments to verify the outstanding performance of the controller. The experimental results show that the system can effectively suppress the disturbance and hysteresis, and the accuracy of system is less than 1 μrad. Compared to traditional ADRC and without ILC compensation, the improved ADRC-ILC strategy improves accuracy by 27% and 31%. Since this controller implementation does not require a hysteresis model, it can be also applied to other hysteresis plants.

Our next work is to eliminate the time delay mainly caused by CCD and improve the spot position solution algorithm. Kalman filter algorithm can be used to compensate the time delay by predicting target position and using predictive values and measured values to compensate time delay, which is our future research interest.

Acknowledgment

The authors would like to thank the anonymous reviewers for their valuable suggestions.

References

[1] S. Arnon and N. S. Kopeika, "Vibration noise control in laser satellite communication," *Proc. SPIE*, vol. 4365, pp. 188–194, 2001.
[2] R. W. Cochran and R. H. Vassar, "Fast-steering mirrors in optical control systems," *Proc. SPIE*, vol. 1303, pp. 245–251, 1990.
[3] Y. Kaymak, R. Rojas-Cessa, J. Feng, N. Ansari, and M. C. Zhou, "On divergence-angle efficiency of a laser beam in free-space optical communications for high-speed trains," *IEEE Trans. Veh. Technol.*, vol. 66, no. 9, pp. 7677–7687, Sep. 2017.
[4] R. Florentin *et al.*, "Shaping the light amplified in a multimode fiber," *Light, Sci. Appl.*, vol. 6, no. 2, 2017, Art. no. e16208.
[5] Y. Li, S. Tong, L. Liu, and G. Feng, "Adaptive output-feedback control design with prescribed performance for switched nonlinear systems," *Automatica*, vol. 80, pp. 225–231, 2017.
[6] Y. Juqing, D. Wang, and W. Zhou, "Precision laser tracking servo control system for moving target position measurement," *Optik-Int. J. Light Electron Opt.*, vol. 131, pp. 994–1002, 2017.
[7] R. G. Lloyds and A. Ali, "Smith predictor based parallel cascade control strategy for unstable and integrating processes with large time delay," *J. Process Control*, vol. 52, pp. 57–65, 2017.
[8] J. Han, "From PID to active disturbance rejection control," *IEEE Trans. Ind. Electron.*, vol. 56, no. 3, pp. 900–906, Mar. 2009.
[9] B.-Z. Guo, Z.-H. Wu, and H.-C. Zhou, "Active disturbance rejection control approach to output-feedback stabilization of a class of uncertain nonlinear systems subject to stochastic disturbance," *IEEE Trans. Autom. Control*, vol. 61, no. 6, pp. 1613–1618, Jun. 2016.
[10] P. Krishnamurthy and F. Khorrami, "A singular perturbation based global dynamic high gain scaling control design for systems with nonlinear input uncertainties," *IEEE Trans. Autom. Control*, vol. 58, no. 10, pp. 2686–2692, Oct. 2013.
[11] S. Luo, Q. Sun, M. Sun, P. Tan, W. Wu, and H. Sun, "On decoupling trajectory tracking control of unmanned powered parafoil using ADRC-based coupling analysis and dynamic feedforward compensation," *Nonlinear Dyn.(Suppl. C)*, vol. 92, pp. 1619–1635, 2018.
[12] L. Shengquan, J. Li, and Y. Mo, "Piezoelectric multimode vibration control for stiffened plate using ADRC-based acceleration compensation," *IEEE Trans. Ind. Electron.*, vol. 61, no. 12, pp. 6892–6902, Dec. 2014.
[13] G. Zhiqiang, "Scaling and bandwidth-parameterization based controller tuning," in *Proc. IEEE Amer. Control Conf.*, 2003, pp. 4989–4996.
[14] Y. Jianyong and W. Deng, "Active disturbance rejection adaptive control of hydraulic servo systems," *IEEE Trans. Ind. Electron.*, vol. 64, no. 10, pp. 8023–8032, Oct. 2017.
[15] T.-T. Jiang, C. Huang, and L. Guo, "Control of uncertain nonlinear systems based on observers and estimators," *Automatica*, vol. 59, pp. 35–47, 2015.
[16] Y.-C. Huang and D.-Y. Lin, "Ultra-fine tracking control on piezoelectric actuated motion stage using piezoelectric hysteretic model," *Asian J. Control*, vol. 6, no. 2, pp. 208–216, 2004.
[17] Z. Li, X. Zhang, C.-Y. Su, and T. Chai, "Nonlinear control of systems preceded by Preisach hysteresis description: A prescribed adaptive control approach," *IEEE Trans. Control Syst. Technol.*, vol. 24, no. 2, pp. 451–460, Mar. 2016.
[18] M. Norrlof, "An adaptive iterative learning control algorithm with experiments on an industrial robot," *IEEE Trans. Robot. Autom.*, vol. 18, no. 2, pp. 245–251, Apr. 2002.
[19] D.-R. Yang, K.-S. Lee, H.-J. Ahn, and J.-H. Lee, "Experimental application of a quadratic optimal iterative learning control method for control of wafer temperature uniformity in rapid thermal processing," *IEEE Trans. Semicond. Manuf.*, vol. 16, no. 1, pp. 36–44, Feb. 2003.
[20] S. Garimella and K. Srinivasan, "Application of iterative learning control to coil-to-coil control in rolling," *IEEE Trans. Control Syst. Technol.*, vol. 6, no. 2, pp. 281–293, Mar. 1998.
[21] S.-A. Saab, "A stochastic iterative learning control algorithm with application to an induction motor," *Int. J. Control*, vol. 77, no. 2, pp. 144–163, 2004.
[22] C.-V. Giessen, Q. Zou, and S. Devasia, "Inversion-based precision positioning of inertial reaction devices," in *Proc. 2004 Amer. Control Conf.*, 2004, pp. 3788–3793.
[23] C.-T. Abdallah, V.-S. Soulian, and E. Schamiloglu, "Toward 'smart tubes' using iterative learning control," *IEEE Trans. Plasma Sci.*, vol. 26, no. 3, pp. 905–911, 1998.
[24] Y. Chen, C. Wen, J.-X. Xu, and M. Sun, "High-order iterative learning identification of projectile's aerodynamic drag coefficient curve from radar measured velocity data," *IEEE Trans. Control Syst. Technol.*, vol. 6, no. 4, pp. 563–570, Jul. 1998.
[25] K.-K. Leang and S. Devasia, "Design of hysteresis-compensating iterative learning control for piezo-positioners: Application to atomic force microscopes," *Mechatronics*, vol. 16, no. 3/4, pp. 141–158, 2006.
[26] Y. Wu and Q. Zou, "Iterative control approach to compensate for both the hysteresis and the dynamics effects of piezo actuators," *IEEE Trans. Control Syst. Technol.*, vol. 15, no. 5, pp. 936–944, Sep. 2007.
[27] A. Al-Ghanimi, J. Zheng, and Z. Man, "A fast non-singular terminal sliding mode control based on perturbation estimation for piezoelectric actuators systems," *Int. J. Control*, vol. 90, no. 3, pp. 480–491, 2017.
[28] G. Heinzinger, D. Fenwick, B. Paden, and F. Miyazaki, "Stability of learning control with disturbances and uncertain initial conditions," *IEEE Trans. Autom. Control*, vol. 37, no. 1, pp. 110–114, Jan. 1992.